

Diffusion-inspired time-varying phosphorescent decay in a nanostructured environmentDenis Kislov,^{1,*} Denis Novitsky,^{1,2} Alexey Kadochkin,³ Dmitrii Redka,⁴ Alexander S. Shalin,¹ and Pavel Ginzburg^{5,6}¹*ITMO University, 49 Kronverksky Pr., St. Petersburg 197101, Russia*²*B.I. Stepanov Institute of Physics, National Academy of Sciences of Belarus, 68 Nezavisimosti Avenue, Minsk 220072, Belarus*³*Ulyanovsk State University, Ulyanovsk 432017, Russia*⁴*Saint Petersburg, Electrotechnical University “LETI” (ETU) 5 Prof. Popova Street, St. Petersburg 197376, Russia*⁵*Center for Photonics and 2D Materials, Moscow Institute of Physics and Technology, Dolgoprudny 141700, Russia*⁶*Tel Aviv University, Ramat Aviv, Tel Aviv 69978, Israel*

(Received 1 October 2019; published 22 January 2020)

Structured environment controls dynamics of light-matter interaction processes via modified local density of electromagnetic states. In typical scenarios, where nanosecond-scale fluorescent processes are involved, mechanical conformational changes of the environment during the interaction processes can be safely neglected. However, slow decaying phosphorescent complexes (e.g., lanthanides) can efficiently probe micro- and millisecond scale motion via near-field interactions with nearby structures. As the result, lifetime statistics can inherit information about nanoscale mechanical motion. Here we study light-matter interaction dynamics of phosphorescent dyes, diffusing in a proximity of a plasmonic nanoantenna. The interplay between time-varying Purcell enhancement and stochastic motion of molecules is considered via a modified diffusion equation, and collective decay phenomena is analysed. Fluid properties, such as local temperature and diffusivity, are mapped on phosphorescent lifetime distribution and then extracted with the help of inverse Laplace transformation. The presented photonic platform enables performing contactless all-optical thermometry and diffusion measurements, paving a way for a range of possible applications. In particular, detailed studies of nanofluidic processes in lab-on-a-chip devices, challenging for analysis with other optical methods, can be performed with time-dependent phosphorescence.

DOI: [10.1103/PhysRevB.101.035420](https://doi.org/10.1103/PhysRevB.101.035420)**I. INTRODUCTION**

Light-matter interaction processes strongly depend on both internal structure of quantum systems and surrounding environments [1]. While the first factor in a vast majority of scenarios is pre-defined by nature, the latter one can be modified by carefully designed nanostructuring [2–6]. Purcell enhancement of spontaneous emission rates with plasmonic nanoantennae is one among prominent examples of tailoring first-order light-matter interaction, e.g., Refs. [7,8]. The essence of structuring-inspired manipulation can be understood via local density of electromagnetic states (LDOS), which enter interaction Hamiltonians governing quantum processes of any order [9,10]. LDOS is directly related to a classical Green's function, which allows formulating quantum problems in terms of pure classical electromagnetic quantities.

Common approach to address light-emission processes is based on time-dependent perturbation theory in the case of weak coupling regime, or on the complete solution of dynamic equations in more advanced strong coupling scenarios. In both cases, however, strength of the fundamental interaction parameter is time independent. This approach is well justified in cavity quantum electrodynamics, where the environment is static and does not change during the interaction. In colloidal applications, where a solution of particles can undergo either

ordered or random motion, dynamical changes of the environment can be also neglected under certain and commonly met approximations. For example, fast virtual level assisted non-linear processes and even dipole-allowed nanosecond scale fluorescent decays are orders of magnitude faster than slow microsecond-scale changes in fluidic environment.

In a sharp contrast to dipole-allowed fluorescent transitions, phosphorescent dyes are characterized by micro- and milli-second slow decays, which originate from fundamentally different quantum process – spin flip followed by the photon emission transition. In particular, phosphorescent (e.g., Ref. [11]) and rare earth (e.g., Ref. [12]) luminescent molecules have characteristic decay times in a range of micro and even milliseconds scales. Those properties can be employed for different imaging techniques, such as gated photoluminescence microscopy [13], and also can be affected by nanostructuring [14–17]. In terms of fundamental light-matter interaction processes, phosphorescent timescales can be comparable with conformational changes inside colloidal environment. For example, a spherical molecule in water at room temperature has an average drift of several hundreds of nm during the time period of 100 μ s. This nanoscale displacement between an emitter and a nanoantenna is enough to dramatically change the decay rate, as it will be shown hereafter. It is worth noting that conformational changes are still significantly slower than the optical carrier frequency and allow applying time-scale separation approach for the theoretical treatment. This approach has been recently applied

*denis.a.kislov@gmail.com

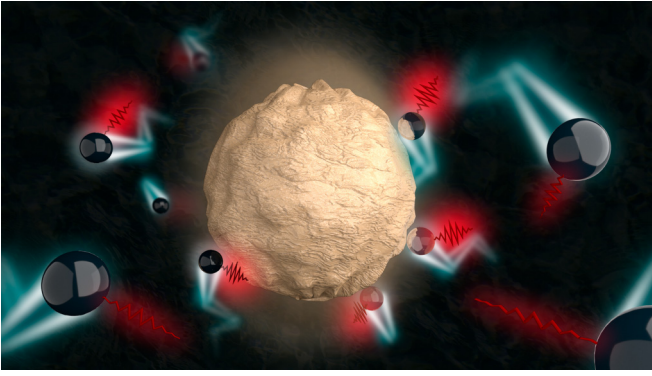


FIG. 1. The schematics of the system–diffusion of slow-decaying phosphorescent dyes next to a resonant nanoantenna.

to velocimetry mapping with phosphorescent emitters [18] and for analysis of rotational micro-Doppler effects [19,20].

Here we develop a theoretical framework for treating diffusion processes of slow-decaying phosphorescent compounds in a solution of resonant optical antennae (Fig. 1). An assembly of emitters, dissolved in a liquid mixed with metal nanoparticles, is pumped with an external illumination. Slow-decaying dyes diffuse in the vicinity of resonating nanoparticles and change their emission on the timescale, comparable with the spontaneous decay. As the result of this interaction, the information on the fluid dynamics is imprinted in the photon statistics.

The manuscript is organized as follows: the basic diffusion model with an additional decay term associated with the position-dependent Purcell effect is introduced in Sec. II. Contrary to traditional description of diffusion processes, the overall number of excited emitters is kept as a variable. Orientation-averaged and position-dependent Purcell factor is calculated next. The analysis is based on the evaluation of classical Green’s functions via Mie series expansion. Solution of the diffusion equation with the position-dependent Purcell-driven decay factor comes as the main result in Sec. II D, followed by the conclusions in Sec. IV.

II. THEORETICAL FORMALISM

A. Diffusion model

The proposed diffusion model describes the density of excited and time-decaying molecules, undergoing Brownian motion in a proximity of metal or dielectric nanoparticles (Fig. 1). Since the later objects have significantly higher mass, they can be assumed to be static during the interaction (however, the reference frame can be linked directly to the resonator, which is static in its rest frame). The concentration of excited molecules is $n(\mathbf{r}, t)$ and it depends not only on the diffusion in a solvent, but also on time via Purcell-enhanced interactions with a nearby nanoantenna. This position-dependent decay rate can be written as $\gamma(\mathbf{r}) = \gamma_0 F(\mathbf{r})$, where $F(\mathbf{r})$ is the Purcell factor and \mathbf{r} stays for the distance between the nanoparticle and the excited molecule. In free space, without a particle present, the characteristic decay time is $\tau_0 = 1/\gamma_0$. For lanthanide complexes it can vary from

μs to ms depending on an internal structure and surrounding solvent, which can quench the radiation.

The diffusion equation for this type of a process can be written as

$$\frac{\partial n}{\partial t} = D\Delta n - \gamma(\mathbf{r})n, \quad (1)$$

where D is the diffusion coefficient of phosphorescent molecules. Purcell effect introduces an additional spatially dependent decay channel. Diffusion coefficient (D) generally depends on temperature and other parameters of an environment, which can be related to each other via Stokes–Einstein relation:

$$\frac{D_{T_1}}{D_{T_2}} = \frac{T_1 \mu_{T_2}}{T_2 \mu_{T_1}}, \quad (2)$$

where μ is a solvent’s dynamic viscosity and subindices correspond to different local temperatures [21]. This dependence can provide a new methodology for local temperature sensing via Purcell-effect-induced luminescence modification, as it will be shown with forthcoming analysis.

Hereinafter, the model will concentrate on the interaction dynamics with a single spherical particle by assuming radial symmetry of the entire scenario. It means that the pumping mechanism is also isotropic (unpolarized) and it induces a spatially dependent excitation of molecules in the region under consideration. While the antenna effect for pump can be also introduced, here for the sake of simplicity we assume a Gaussian initial distribution of the form $n(r, 0) = n_0 e^{-2r^2/R_b^2}$, where R_b is the waist radius of a tightly focused pump laser beam. Under the simplifying conditions, we can neglect the angular dependence of concentration and recast Eq. (1) in spherical coordinates by leaving only the radial component:

$$\frac{\partial n}{\partial t} = D \frac{\partial^2 n}{\partial r^2} + 2 \frac{D}{r} \frac{\partial n}{\partial r} - \gamma(r)n. \quad (3)$$

We will solve Eq. (3) numerically in a range of r from the radius of the nanoparticle (a) to a certain value $R \gg a$. This allows us to set the boundary conditions as an absence of molecular flow near the surface and far away from the nanoparticle $\frac{\partial n(0,t)}{\partial r} = \frac{\partial n(R,t)}{\partial r} = 0$. This assumption relies on relatively low density of nanoparticles in the liquid. To obtain the solution of Eq. (3), position-dependent Purcell Factor should be estimated, which will be done next.

While the proposed model assumes low concentration of plasmonic nanoparticles, it can be extended to scenarios that are more complex. Increase in the concentration can lead to emergence of several effects. For example, dye molecule can drift from one resonator to another—in this case, boundary conditions for Eq. (3) should be modified. For dense nanoparticle solutions, antenna-antenna interaction start playing a role, giving rise to collective modes. In this case, LDOS based on Green’s functions formalism should be revised. The general model for the case of high concentration should address both of the beforehand mentioned aspects and cannot utilize the radial symmetry, assumed for deriving Eq. (3). To justify the low concentration assumption, the volumetric fraction of gold nanoparticles should be less than a single one per focal volume of a collecting objective. Also, the mean-squared displacement of diffusing molecules during

their decay time should be smaller than an averaged spacing between gold nanoparticles. Furthermore, high concentration of emitting molecules can lead to additional decay channels (concentration quenching), which can complicate the overall dynamics beyond the proposed model. Optimal concentration values around $100 \mu\text{M}$ [22] and other beforehand mentioned conditions can be met in a possible experimental realization.

B. Position and orientation averaged Purcell enhancement

Electromagnetic Green's function of a radiating dipole next to spherical dielectric particle has a closed form analytical solution based on Mie theory. This allows to obtain analytical expressions for Purcell factor, describing the enhancement of spontaneous emission rates in the vicinity of nanoparticles as follows [23,24]:

$$\begin{aligned}
 F_{\perp}^{\text{rad}}(r) &= \frac{3}{2} \sum_{m=1}^{\infty} m(m+1)(2m+1) \\
 &\times \left| \frac{\psi_m(kr\sqrt{\varepsilon_d})}{(kr\sqrt{\varepsilon_d})^2} + A_m \frac{\xi_m(kr\sqrt{\varepsilon_d})}{(kr\sqrt{\varepsilon_d})^2} \right|^2, \\
 F_{\parallel}^{\text{rad}}(r) &= \frac{3}{4} \sum_{m=1}^{\infty} (2m+1) \left(\left| \frac{\psi_m(kr\sqrt{\varepsilon_d})}{kr\sqrt{\varepsilon_d}} + B_m \frac{\xi_m(kr\sqrt{\varepsilon_d})}{kr\sqrt{\varepsilon_d}} \right|^2 \right. \\
 &\left. + \left| \frac{\psi'_m(kr\sqrt{\varepsilon_d})}{kr\sqrt{\varepsilon_d}} + A_m \frac{\xi'_m(kr\sqrt{\varepsilon_d})}{kr\sqrt{\varepsilon_d}} \right|^2 \right), \quad (4)
 \end{aligned}$$

where F_{\perp}^{rad} and $F_{\parallel}^{\text{rad}}$ stay for *radiative* enhancement of the emission in the case, when the dipole moment of a molecule is either perpendicular or parallel to the nanosphere surface. In the case, when the molecules are randomly oriented in respect to the sphere, the average enhancement is given by $F^{\text{rad}}(r) = \frac{2}{3}F_{\parallel}^{\text{rad}}(r) + \frac{1}{3}F_{\perp}^{\text{rad}}(r)$. Corresponding *total* rate enhancements are given by

$$\begin{aligned}
 F_{\parallel}^{\text{tot}}(r) &= 1 + \frac{3}{4} \sum_{m=1}^{\infty} (2m+1) \\
 &\times \text{Re} \left[B_m \left(\frac{\xi_m(kr\sqrt{\varepsilon_d})}{kr\sqrt{\varepsilon_d}} \right)^2 + A_m \left(\frac{\xi'_m(kr\sqrt{\varepsilon_d})}{kr\sqrt{\varepsilon_d}} \right)^2 \right], \\
 F_{\perp}^{\text{tot}}(r) &= 1 + \frac{3}{2} \sum_{m=1}^{\infty} m(m+1)(2m+1) \\
 &\times \text{Re} \left[A_m \left(\frac{\xi_m(kr\sqrt{\varepsilon_d})}{(kr\sqrt{\varepsilon_d})^2} \right)^2 \right]. \quad (5)
 \end{aligned}$$

In Eqs. (4) and (5) ε_d is the dielectric permittivity of the environment, k - wavenumber in vacuum, A_m and B_m are Mie coefficients (widely used notions have been used [23,24]), m - number of multipole terms, $\psi_m(x) = x j_m(x)$, $\xi_m(x) = x h_m^{(1)}(x)$, where $j_m(x)$ and $h_m^{(1)}(x)$ are, respectively, spherical Bessel and Hankel functions of the first kind.

Radiative and nonradiative enhancements should be distinguished, as they influence the light-matter interaction in different ways. Total radiative lifetime governs the decay dynamics, while the radiative contribution is responsible for

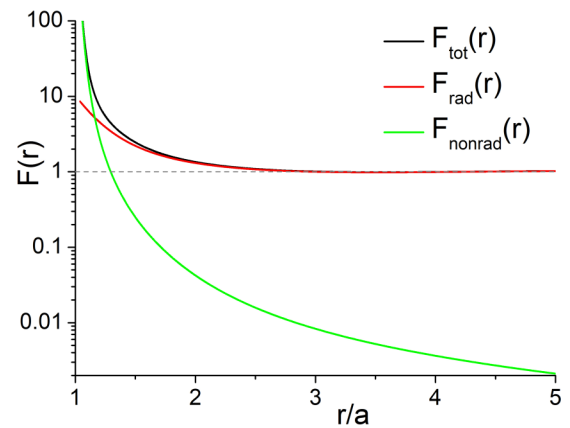


FIG. 2. Purcell enhancement next to a gold (50-nm-radius) nanoparticle. Orientation-averaged total, radiative, and nonradiative enhancements (black, red, and green lines, respectively) as a function of the normalized distance (to the particle's radius) between the dipole and particle's surface. Detailed parameters are given in the main text.

a number of photons detected at the far field. The difference between radiative and total rates is the result of losses within the particle [25]. While in a majority of optoelectronic applications only the radiative enhancement is a factor for maximization, our diffusion model requires the knowledge of the total decay rate. The information about local properties of the fluid, however, can be analyzed via collecting emitted photons. Separation into radiative and nonradiative channels, based on Green's functions formalism, can be also preformed [26].

Radiative and total enhancements are plotted as the function of the distance between the emitter and the gold nanoparticle (Fig. 2). The following typical parameters have been used—the radius of the spherical particle is 50 nm, the optical properties of gold were taken from [27]. The phosphorescent emission central wavelength is 690 nm. It can be seen that nonradiative channels prevail the decay dynamics in the close proximity of the particle, while at distances larger than 100 nm the influence of the particle is minor, and Purcell enhancement approaches unity (no enhancement). Qualitatively, it means that far-situated fluorophores will contribute to the background radiation and will decay with the rate of γ_0 . Those contributions can be factorized by applying lifetime distribution post-processing techniques [28]. The most relevant region for observing the diffusion dynamics via photon counting is situated at distances of 20–100 nm from the nanoparticle surface.

C. Temperature dependence of the diffusion coefficient

Taking into account the spatial distribution of the Purcell enhancement and low density of the dissolved nanoparticles, electromagnetic coupling between neighboring nanoantennas can be ignored. Furthermore, contributions of the emitters situated far apart from the particle are neglected, since their lifetimes are unmodified during the diffusion process, as it was previously discussed.

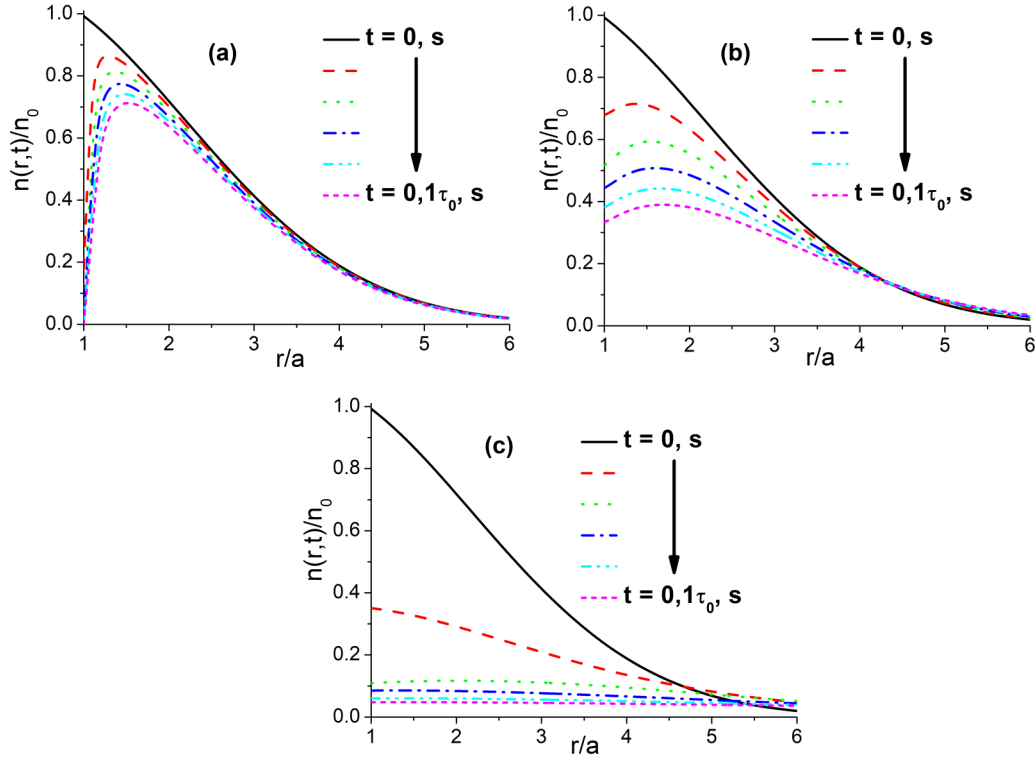


FIG. 3. Radial distribution of excited dye molecules density in a vicinity of the particle. Different times, elapsed from the pump pulse are represented with color lines (in captions—[0 : 6 : 0.1 τ_0] the interval is equidistantly divided into six sections). Diffusion coefficients (D [$\mu\text{m}^2/\text{ms}$]) are: (a) 0, (b) 0.2, (c) 1.6. Other parameters: $a = 50$ nm, $R_b = 4.8a$, $\tau_0 = 300$ μs .

The diffusion coefficient of emitters is given by the Stokes-Einstein relation assuming spherical shapes of the molecules and low Reynolds numbers, which are justified in the case of nanoscale objects dissolved in water [29]:

$$D(T) = \frac{k_B T}{6\pi\mu(T)R_{\text{mol}}}, \quad (6)$$

where μ is the dynamical viscosity of the solvent, T is absolute temperature, and R_{mol} is the radius of the light-emitting complex. $R_{\text{mol}} \approx 0.5$ -1 nm for the molecules, which are discussed here [29]. There are empirical models relating dynamical viscosity and local temperature. For example, distilled water obeys $\mu(T) = A_0 10^{B_0/T - C_0}$, where $A_0 = 2.4 \times 10^{-5}$ Pa s, $B_0 = 247.8$ K и $C_0 = 140$ K. In this case, the diffusion coefficient for a range of organic compounds (e.g., eosin, rose bengal, erythrosine), which possess relevant phosphorescent properties [30], will fall in the following range: $0.2 \div 1.6$ $\mu\text{m}^2/\text{ms}$ (from 273 to 373 K).

D. Analysis of the diffusion-inspired emission dynamics

Having the values of the diffusion coefficient and the position-dependent Purcell factor, the entire model can be solved now. Figure 3 shows the density of the excited molecules as a function of the distance from the particle at different instances of time. Color lines correspond to different times elapsed from the instance of the pulsed pump excitation.

It can be seen from Fig. 3 that when the diffusion coefficient is very small (panel a) the population of excited dyes drops down fast next to the particle and there is no

Brownian inflow towards it. However, when the diffusion is efficient, slow decaying molecules (unaffected by Purcell enhancement) flow in and start sensing the presence of the antenna. As the result, they become decaying faster. This dynamical behavior is clearly seen by comparing panels a, b, and c. The diffusion kinetics has a direct replica on the lifetime distribution, which can be measured at the far field.

Intensity, collected at the far field, has the following time dependence:

$$I(t) \sim \int_a^{R_{\text{collection}}} \int_0^\pi \int_0^{2\pi} F^{\text{rad}}(r) \gamma_0 n(r, t) r^2 \sin^2(\vartheta) dr d\vartheta d\varphi. \quad (7)$$

$R_{\text{collection}}$ here corresponds to the focal volume of a collecting objective and it is supposed to be much larger than the spot size of the exciting beam R_b (this assumption does not affect the main result, however). Note that the time dependence solely originates from $n(r, t)$. While $n(r, t)$ is governed by the total decay rate, the emitted intensity in Eq. (7) also depends explicitly on the radiative Purcell enhancement. Figure 4(a) demonstrates the time-dependent intensity decay for different values of the diffusion constant. It is clearly seen that in the chosen range of parameters the intensity drops faster with the increase of the diffusivity. When the molecules are randomly moving around the antenna, they have larger probability to be found in its vicinity and, as a result, they experience larger Purcell enhancement.

The kinetics of the collected intensity can be used as a tool for diffusion and, hence, temperature detection. To demonstrate this, we apply the inverse Laplace transformation

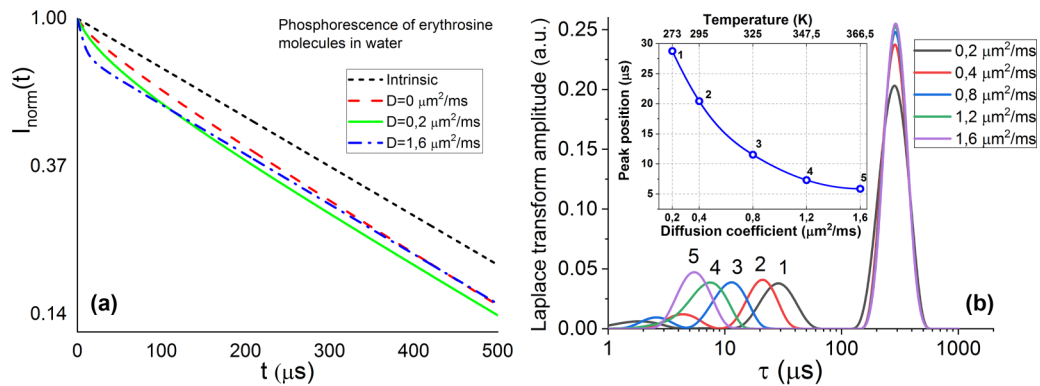


FIG. 4. (a) Normalized intensity (log-scale) decay of the dye molecules in a vicinity of the particle for different diffusion coefficient values: Intrinsic phosphorescence of erythrosine molecules in water (no particle present) and with the particle present for D [$\mu\text{m}^2/\text{ms}$] = 0, 0.2, and 1.6. (b) Lifetime distribution analysis of the collected luminescence signal. Color lines correspond to different diffusion coefficients and, hence, temperatures. The inset shows the position of the secondary (numbered) peak as the function of the diffusion coefficient. The decay time is derived from the regularized inverse Laplace transformation. The radius of the collecting objective focal volume is $R_{\text{collection}} = 10a$.

on the function $I(t)$ given by Eq. (7). Namely, the intensity can be represented as

$$I(t) = \int_0^\infty g(s)e^{-st} ds, \quad (8)$$

where $s = 1/\tau$ is the inverse relaxation time. We solve this equation using the numerical approach similar to that reported in Ref. [28] and get the distribution $g(s)$ for different exponential contributions to the total luminescence kinetics. The result is shown in Fig. 4(b), where the nonexponential response of the system is clearly seen. The right strongest peak corresponds to the free-space relaxation time of the molecules ($\tau_0 = 300 \mu\text{s}$). The secondary peak on the left is associated to the Purcell effect and contains the information on the diffusion characteristics. Indeed, it is seen that the increase in the diffusion coefficient results in further shift of this secondary peak towards shorter lifetimes due to increasing probability for molecules to approach to the metal nanoparticle. The position of this peak as a function of the diffusion coefficient and, consequently the temperature, is shown in the inset. Therefore, it becomes possible to measure temperature and diffusion coefficient in a liquid via the proposed photonic contactless design. This pronounced dependence of the optical signature of phosphorescent molecules on surroundings can be extremely useful for remote all-optical temperature control.

III. OUTLOOK

Quite a few spectroscopic methods have been developed for thermometry applications. For example, different types of vacancies in nanodiamonds were shown to serve as an excellent platform for high-resolution temperature mapping [31,32]. Micro-photoluminescence measurements of quantum well structures can be used for mapping cryogenic temperatures [33]. Quite a few proposals and demonstrations have been developed for measuring temperatures in microchannels [34–37] and diffusion coefficients of reagents in microfluidic cells [38,39]. Monitoring and control of fluid properties, such as temperatures and viscosities, as well as associated mass transfer processes (including diffusion), is crucial in many biochemical, biological and medical applications.

For example, several degrees deviations significantly affect efficiencies of polymerase chain reactions [40], the heating mode in the Reimer–Tiemann reaction [41], crystallization process of quantum dots formation [42], and many others. Environmental control is especially important for protein-based biotherapeutic drugs, which are very sensitive to temperature fluctuations (for example, insulin [43] and monoclonal antibodies), which are a new class of biotherapeutic drugs used to treat various diseases, such as autoimmune diseases and cancer [44,45]. Therefore, microanalysis methods provide significant benefits for characterizing the degradation of such drugs, because native protein solutions have different viscosities in comparison to degraded samples [46,47].

Our approach for measuring the diffusion coefficient and temperature offers flexible solutions for the beforehand mentioned applications. Under experimental constrains, resonant metal nanoparticles can be mixed with a fluid within a channel. However, nanoantennae array can be directly deposited on channel boundaries (e.g., Ref. [48]). Analyte solution is then mixed with slow-decaying molecules. Erythrosine, eosin, bengal rose, and rare-earth metal ion complexes are among the candidates that can be employed in the experiment. This versatility provides flexibility in choosing certain spectral range for analysis as well as identifying characteristic decay times, most suitable for a desirable range of solvent's viscosity. Relevant concentration, antennae spacing and other conditions, which simplify data interpretation, have been discussed after Eq. (3). High numerical objective should be used for pumping the dyes and for collecting the emission. While time-correlated single photon counting (TCSPC) techniques should be used for retrieving time-dependent intensity decay, slow decaying phosphorescence can be detected with sensitive photodiodes, capable to resolve the signal in time.

IV. CONCLUSIONS

Lab-on-a-chip architectures, capable to accommodate several sensing functions within in a miniature device, is a fast-growing field attracting ever-increasing attention. However, hardware realizations of many important functionalities are often face challenges, especially in cases when nanoscale

resolution is required. Here we developed a novel concept for contactless all-optical temperature and diffusion measurements, which are enabled by dynamic time-dependent Purcell effect in a solution of phosphorescent molecules interfacing resonant nanoantennae. Dynamics of the long lifetime phosphorescent molecules decay is shown to be strongly dependent on the Brownian motion next to a resonator. This special interaction is described with temperature-dependent diffusion coefficient of the surrounding liquid. Subsequently, far-field radiation emitted from diffusing molecules is analyzed via the inverse Laplace transform and exploited to recover local properties of a fluid environment. As the result, an efficient contact-free approach to measure required hydrodynamical characteristics of a liquid in a broad temperature range with

nanoscale spatial resolution is demonstrated. Moreover, the proposed method can utilize biologically compatible compounds demonstrating new capabilities in a variety of lab-on-a-chip realizations and expanding the range of microfluidics applications.

ACKNOWLEDGMENTS

The work has been supported in part by ERC StG “In Motion” and PAZY Foundation. A.S.S. acknowledges the support of the Russian Fund for Basic Research within Projects No. 18-02-00414 and No. 18-52-00005. Numerical simulations of the particles dynamics and lifetimes have been supported by the Russian Science Foundation (Project No. 18-72-10127).

-
- [1] L. Novotny and B. Hecht, *Principles of Nano-Optics*, 2nd ed. (Cambridge University Press, Cambridge, 2012).
- [2] K. V. Baryshnikova, A. Novitsky, A. B. Evlyukhin, and A. S. Shalin, *J. Opt. Soc. Am. B* **34**, D36 (2017).
- [3] P. D. Terekhov, V. E. Babicheva, K. V. Baryshnikova, A. S. Shalin, A. Karabchevsky, and A. B. Evlyukhin, *Phys. Rev. B* **99**, 045424 (2019).
- [4] E. A. Gurvitz, K. S. Ladutenko, P. A. Dergachev, A. B. Evlyukhin, A. E. Miroshnichenko, and A. S. Shalin, *Laser Photonics Rev.* **13**, 1800266 (2019).
- [5] H. K. Shamkhi, K. V. Baryshnikova, A. Sayanskiy, P. Kapitanova, P. D. Terekhov, P. Belov, A. Karabchevsky, A. B. Evlyukhin, Y. Kivshar, and A. S. Shalin, *Phys. Rev. Lett.* **122**, 193905 (2019).
- [6] K. Baryshnikova, D. Filonov, C. Simovski, A. Evlyukhin, A. Kadochkin, E. Nenasheva, P. Ginzburg, and A. S. Shalin, *Phys. Rev. B* **98**, 165419 (2018).
- [7] L. Novotny and N. Van Hulst, *Nat. Photonics* **5**, 83 (2011).
- [8] J. J. Greffet, *Science* **308**, 1561 (2005).
- [9] G. Milburn, *Quantum Optics*, 3rd ed. (Wiley-VCH, Weinheim, Germany, 2012).
- [10] P. Ginzburg, *Rev. Phys.* **1**, 120 (2016).
- [11] K. J. Morris, M. S. Roach, W. Xu, J. N. Demas, and B. A. DeGraff, *Anal. Chem.* **79**, 9310 (2007).
- [12] D. Liu, Z. Wang, H. Yu, and J. You, *Eur. Polym. J.* **45**, 2260 (2009).
- [13] W. A. W. Razali, V. K. A. Sreenivasan, C. Bradac, M. Connor, E. M. Goldys, and A. V. Zvyagin, *J. Biophotonics* **9**, 848 (2016).
- [14] D. J. Roth, P. Ginzburg, L. M. Hirvonen, J. A. Levitt, M. E. Nasir, K. Suhling, D. Richards, V. A. Podolskiy, and A. V. Zayats, *Laser Photon. Rev.* **13**, 1900101 (2019).
- [15] M. G. Kucherenko and D. A. Kislov, *J. Photochem. Photobiol. A Chem.* **354**, 25 (2018).
- [16] S. V. Izmodenova, D. A. Kislov, and M. G. Kucherenko, *Colloid J.* **76**, 683 (2014).
- [17] D. A. Kislov and M. G. Kucherenko, *Opt. Spectrosc. (English Transl. Opt. i Spektrosk.)* **117**, 784 (2014).
- [18] A. S. Kadochkin, I. I. Shishkin, A. S. Shalin, and P. Ginzburg, *Laser Photonics Rev.* **12**, 1800042 (2018).
- [19] V. Kozlov, D. Filonov, Y. Yankelevich, and P. Ginzburg, *J. Quant. Spectrosc. Radiat. Transf.* **190**, 7 (2017).
- [20] D. Filonov, B. Z. Steinberg, and P. Ginzburg, *Phys. Rev. B* **95**, 235139 (2017).
- [21] I. Shishkin, T. Alon, R. Dagan, and P. Ginzburg, *MRS Adv.* **2**, 2391 (2017).
- [22] D. Ross, M. Gaitan, and L. E. Locascio, *Anal. Chem.* **73**, 4117 (2001).
- [23] S. V. Gaponenko, P.-M. Adam, D. V. Guzatov, and A. O. Muravitskaya, *Sci. Rep.* **9**, 7138 (2019).
- [24] D. V. Guzatov, S. V. Vaschenko, V. V. Stankevich, A. Y. Lunevich, Y. F. Glukhov, and S. V. Gaponenko, *J. Phys. Chem. C* **116**, 10723 (2012).
- [25] P. Ginzburg, *Ann. Phys.* **528**, 571 (2016).
- [26] A. N. Poddubny, P. Ginzburg, P. A. Belov, A. V. Zayats, and Y. S. Kivshar, *Phys. Rev. A At. Mol. Opt. Phys.* **86**, 033826 (2012).
- [27] P. B. Johnson and R. W. Christy, *Phys. Rev. B* **6**, 4370 (1972).
- [28] P. Ginzburg, D. J. Roth, M. E. Nasir, P. Segovia, A. V. Krasavin, J. Levitt, L. M. Hirvonen, B. Wells, K. Suhling, D. Richards, V. A. Podolskiy, and A. V. Zayats, *Light Sci. Appl.* **6**, e16273 (2017).
- [29] Y. Chenyakin, A. D. Ullmann, E. Evoy, L. Renbaum-Wolff, S. Kamal, and K. A. Bertram, *Atmos. Chem. Phys.* **17**, 2423 (2017).
- [30] A. Penzkofer, A. Tyagi, E. Slyusareva, and A. Szykh, *Chem. Phys.* **378**, 58 (2010).
- [31] X. Meng, S. Liu, J. I. Dadap, and R. M. Osgood, *Phys. Rev. Mater.* **1**, 015202 (2017).
- [32] C. Bradac, W. Gao, J. Forneris, M. E. Trusheim, and I. Aharonovich, *Nat. Commun.* **10**, 5625 (2019).
- [33] V. S. Krivobok, S. N. Nikolaev, E. E. Onishchenko, A. A. Pruchkina, S. I. Chentsov, A. Y. Klokov, S. V. Sorokin, and I. V. Sedova, *J. Lumin.* **213**, 273 (2019).
- [34] G. D. Brinatti Vazquez, O. E. Martínez, and J. Martín Cabaleiro, *Appl. Opt.* **58**, 5556 (2019).
- [35] J. Wu, T. Y. Kwok, X. Li, W. Cao, Y. Wang, J. Huang, Y. Hong, D. Zhang, and W. Wen, *Sci. Rep.* **3**, 3321 (2013).
- [36] R. G. Geitenbeek, J. C. Vollenbroek, H. M. H. Weijertze, C. B. M. Tregouet, A. E. Nieuwelink, C. L. Kennedy, B. M. Weckhuysen, D. Lohse, A. Van Blaaderen, A. Van Den Berg, M. Odijk, and A. Meijerink, *Lab Chip* **19**, 1236 (2019).
- [37] I. Wegrzyn, A. Ainla, G. D. M. Jeffries, and A. Jesorka, *Sensors (Switzerland)* **13**, 4289 (2013).

- [38] C. T. Culbertson, S. C. Jacobson, and J. Michael Ramsey, *Talanta* **56**, 365 (2002).
- [39] C. Peters, L. Wolff, S. Haase, J. Thien, T. Brands, H. J. Koß, and A. Bardow, *Lab Chip* **17**, 2768 (2017).
- [40] A. M. Chaudhari, T. M. Woudenberg, M. Albin, and K. E. Goodson, *J. Microelectromech. Syst.* **7**, 345 (1998).
- [41] A. Iles, R. Fortt, and A. J. de Mello, *Lab Chip* **5**, 540 (2005).
- [42] E. M. Chan, A. P. Alivisatos, and R. A. Mathies, *J. Am. Chem. Soc.* **127**, 13854 (2005).
- [43] J. Brange and L. Langkjær, in *Pharmaceutical Biotechnology* (Springer, Berlin, 1993), pp. 315–350.
- [44] A. Vennepureddy, P. Singh, R. Rastogi, J. Atallah, and T. Terjanian, *J. Oncol. Pharm. Pract.* **23**, 525 (2017).
- [45] V. de Zwart, S. C. Gouw, and F. A. Meyer-Wentrup, *Cochrane Database Syst. Rev.* **1**, CD011181 (2016).
- [46] L. L. Josephson, E. M. Furst, and W. J. Galush, *J. Rheol. (N.Y.)* **60**, 531 (2016).
- [47] J. A. Pathak, R. R. Sologuren, and R. Narwal, *Biophys. J.* **104**, 913 (2013).
- [48] H. Markovich, I. I. Shishkin, N. Hendler, and P. Ginzburg, *Nano Lett.* **18**, 5024 (2018).